Pressure-induced gap closing and metallization of $MoSe_2$ and $MoTe_2$

Michaela Rifliková,[1,2] Roman Martoňák,[1,*] and Erio Tosatti[3,4]

[1]*Department of Experimental Physics, Comenius University, Mlynská Dolina F2, 842 48 Bratislava, Slovakia*

[2]*Institute of Electrical Engineering, Slovak Academy of Sciences, Dúbravská cesta 9, 841 04 Bratislava, Slovakia*

[3]*International School for Advanced Studies (SISSA) and CNR-IOM Democritos, Via Bonomea 265, I-34136 Trieste, Italy*

[4]*The Abdus Salam International Centre for Theoretical Physics (ICTP), Strada Costiera 11, I-34151 Trieste, Italy*

(Received 16 January 2014; revised manuscript received 28 May 2014; published 10 July 2014)

Layered molybdenum dichalchogenides are semiconductors whose gap is controlled by delicate interlayer interactions. The gap tends to drop together with the interlayer distance, suggesting collapse and metallization under pressure. We predict, based on first-principles calculations, that layered semiconductors $2H_c$-$MoSe_2$ and $2H_c$-$MoTe_2$ should undergo metallization at pressures between 28 and 40 GPa ($MoSe_2$) and 13 and 19 GPa ($MoTe_2$). Unlike MoS_2 where a $2H_c \rightarrow 2H_a$ layer-sliding transition is known to take place, these two materials appear to preserve the original $2H_c$ layered structure at least up to 100 GPa and to increasingly resist lubric layer sliding under pressure. Similar to metallized MoS_2, they are predicted to exhibit a low density of states at the Fermi level, and presumably very modest superconducting temperatures, if any. We also study the β-$MoTe_2$ structure, metastable with a higher enthalpy than $2H_c$-$MoTe_2$. Despite its ready semimetallic and (weakly) superconducting character already at zero pressure, metallicity is not expected to increase dramatically with pressure.

DOI: 10.1103/PhysRevB.90.035108 PACS number(s): 61.50.Ks, 62.50.−p, 71.30.+h, 72.80.Ga

I. INTRODUCTION

Transition-metal dichalchogenides (TMDs) are well-known and long-characterized compounds [1,2]. They possess a layered crystal structure consisting of MX_2 (M: transition metal; X: chalcogen) XMX composite triatomic layers, where the transition-metal monoatomic layer is sandwiched between two layers of chalcogen atoms. The layers consisting of covalently bonded atoms are only weakly coupled by partly van der Waals interactions, resulting in highly anisotropic properties. By analogy with graphite, their structure based on independently stable, relatively unreactive triatomic layers which can be mutually sheared is probably related to the functioning of some materials, such as MoS_2 and $MoSe_2$, as lubricants. At the same time, it opens the way to a rich polytypism, due to various possible relative stackings of the layers. Much initial interest in bulk materials has been driven by their electronic properties, including insulator, semiconductor, metal, charge-density-wave (CDW) material, and superconductor—properties that can also be modified by intercalation. More recently, the focus has shifted to the exfoliated monolayers, similar to graphene. Owing to removal of interlayer interactions, a monolayer, unlike the bulk material, has a larger and direct band gap, features which in MoS_2 make it of interest for optoelectronics [3–8].

On the opposite front, it is possible to modify the properties of bulk TMDs by external hydrostatic pressure, which can, in principle, cause structural as well as electronic phase transitions. In Ref. [9], $2H_c$-$MoSe_2$ was compressed up to 35.9 GPa and studied by x-ray diffraction, but no structural transition was reported. At normal conditions, MoS_2, $MoSe_2$, and $MoTe_2$ are semiconductors with indirect energy gaps of about 1.29, 1.1, and 1.0 eV, respectively.

The behavior of MoS_2 under pressure is now well understood. Its resistivity decreases with pressure [10], suggesting possible metallization at high pressure. While that possibility is confirmed by calculations [11], it was also theoretically found that the initial $2H_c$ structure (hexagonal, space group $P6_3/mmc$) at zero pressure should undergo, near 20 GPa, a pressure-induced structural transition to $2H_a$ (the same space group $P6_3/mmc$), which is the structure typical of, e.g., NbS_2 (Fig. 1). That result explained some previously mysterious x-ray diffraction evidence [12] and Raman scattering data [13], and was also recently confirmed experimentally [14]. Both MoS_2 phases were predicted to metallize at the same pressure region where the structural transition takes place, i.e., $2H_c$ at 25 GPa and $2H_a$ at 20 GPa—an electronic result not yet investigated by experiments.

The behavior of MoS_2 suggests the possibility that pressure-induced gap closing similar to that of MoS_2 might occur in the similar materials $MoSe_2$ and $MoTe_2$. The experimental electrical resistivity of $MoSe_2$ under pressure appears to be controversial. In Ref. [10], a sudden resistivity drop was found at 4 GPa, with no interpretation provided. In more recent work, Ref. [15] resistivity was studied up to 8 GPa and was found to decrease smoothly upon compression with no sudden drop.

For the next member of this group, $MoTe_2$, also semiconducting in its $2H_c$ room-temperature, zero-pressure stable form (α-$MoTe_2$), the pressure dependence of resistivity is not known. High temperature is known to induce a structural transition to a new β-$MoTe_2$ phase [16] (monoclinic, space group $P2_1/m$), which is still a layered structure with additional modulation of structure inside the layers, so that the Mo atoms now present a distorted octahedral coordination rather than the trigonal prismatic one of $2H_c$ [17]. Interestingly, the β phase is metallic at zero pressure. The transition from α- to β-$MoTe_2$ occurs by raising the temperature to 900 °C [16], but the new structure survives in a metastable state upon cooling down to room temperature—or even to cryogenic temperature where it reportedly shows superconductivity [1]. No high-pressure data appear to be available for either α- or β-$MoTe_2$, and we can therefore only rely on theory concerning their structural and electronic behavior in that regime.

*martonak@fmph.uniba.sk

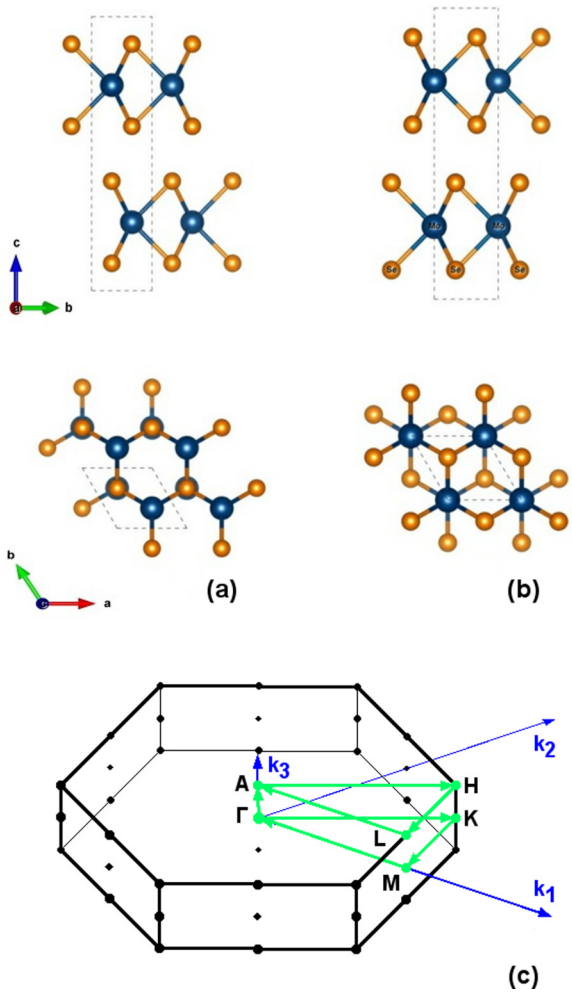

FIG. 1. (Color online) Structures of (a) $2H_c$-$MoSe_2$ and (b) $2H_a$-$MoSe_2$. (c) Brillouin zone for both structures [18].

Here we present first-principles calculations based on density functional theory (DFT) demonstrating the effect of high pressure on bulk transition-metal dichalcogenides $MoSe_2$ and $MoTe_2$, focusing both on the evolution of the crystal structure and of electronic properties. We first will describe in the next section the technical details of the DFT calculations. The following section will present our predicted evolution of the crystalline and electronic structure, predicting the absence of structural transformations, which is surprising in view of the initial analogy to MoS_2, and a semiconductor-band overlap metal transition for both $MoSe_2$ and $MoTe_2$ upon compression. After a discussion of similarities and differences with MoS_2, in particular of the similarly poor metallic properties at high pressure, the last section will summarize our findings and draw conclusions.

II. CALCULATION METHOD

We follow the well-established understanding of, and specifically our own fresh experience with [11], layered TMDs. Straight density functional total-energy and structural calculations, which are quite delicate and uncertain at zero pressure due to large effects caused by the otherwise weak long-range interlayer dispersion van der Waals (vdW) forces which are beyond simple DFT, become much more reliable and predictive at high pressures, where vdW corrections become unnecessary. The case of MoS_2 had been particularly instructive in this respect, showing that whereas the calculated zero-pressure c-axis interlayer spacing with the simple Perdew-Burke-Ernzerhof (PBE) [19] exchange-correlation functional (no vdW) was, as expected, larger than experiment, it improved substantially at 5 GPa, turning extremely close to experiment at 10 GPa and upwards. Assuming, as is very reasonable, the same to hold for $MoSe_2$ and $MoTe_2$, we used no vdW correction and restricted our calculations to pressures of 10 GPa and higher, with no attempt to explore the more delicate and less interesting low-pressure region. In order to increase the dependability of our predicted metallization pressures, we also repeated the electronic structure calculations (with PBE optimized structures, which are trustworthy) with the HSE06 functional which, contrary to PBE, overestimates band gaps and therefore metallization pressures too. The HSE06 calculations were used to establish an upper bound to the semiconductor-metal transition pressure. We employed the QUANTUM ESPRESSO package [20] for structural optimization and calculation of electronic properties. We used scalar relativistic pseudopotentials [26] and, similarly to Ref. [11], we employed a PBE exchange-correlation functional [19] with cutoff of 950 eV. For $2H_c$ structures, we used the six-atom unit cell and $17 \times 17 \times 5$ Monkhorst-Pack [21] (MP) k-point sampling grid for relaxations and $24 \times 24 \times 8$ MP grid for electronic density of states (DOS) calculations. For the β-$MoTe_2$ structure, we used the unit cell with 12 atoms and k-point grids $7 \times 15 \times 5$ and $12 \times 24 \times 6$ for relaxation and DOS calculations, respectively. Spin-orbit coupling was not included in the calculation of total energy and structural optimizations, to which it contributes only in second order. We instead carried out test calculations to check the impact of spin orbit on metallization pressures but found it to be also negligible. In all results presented below, spin-orbit interaction is therefore omitted. Hybrid functional calculations employing the HSE06 functional were performed with norm-conserving pseudopotentials [27]. Zero temperature and neglect of zero-point energy contributions were assumed throughout.

A series of PBE calculations was carried out at increasing pressures from 10 GPa upwards, with, at each pressure, a full structural relaxation aimed at identifying the minimum enthalpy structure, its electronic band structure, and their pressure evolution.

III. RESULTS

A. $MoSe_2$

We performed a compression of the $2H_c$-$MoSe_2$ unit cell up to 130 GPa and calculated the pressure dependence of the lattice parameters a (intralayer) and c (interlayer) (Fig. 2). For comparison, we show in the same figure the experimental data extracted from x-ray diffraction patterns in Ref. [9]. As can be seen, the agreement is excellent especially at pressures beyond 15 GPa, which justifies *a posteriori* the use of the PBE functional without vdW corrections, as was also the case in MoS_2 [11].

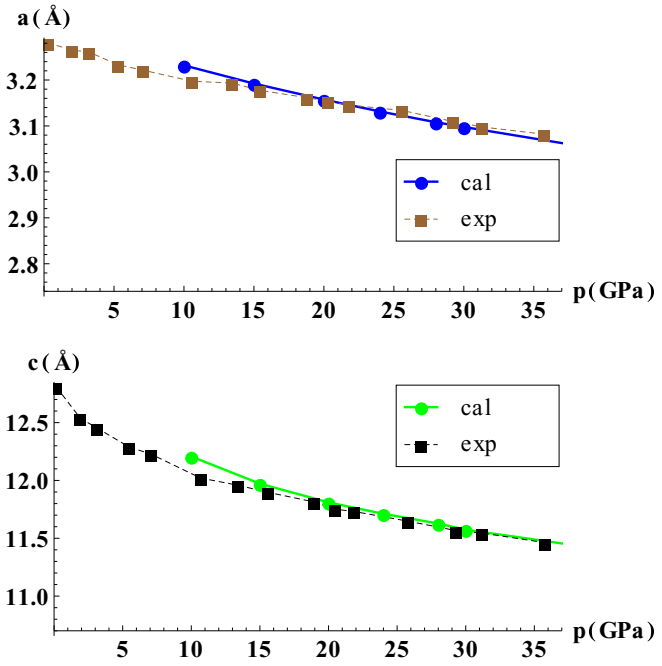

FIG. 2. (Color online) Pressure dependence of the calculated lattice parameters a (upper panel) and c (lower panel) of $2H_c$-$MoSe_2$, together with experimental data from Ref. [9].

The results also agree with experiment in Ref. [9] in $MoSe_2$, indicating no structural changes and the stability of the $2H_c$ zero-pressure structure of $MoSe_2$ at least up to 35.9 GPa. In order to check whether any transition could take place at a higher pressure than this, it would be necessary in the future to conduct some kind of structural search. Limiting ourselves to explore the simple possibility of a transition to the $2H_a$ structure, we calculated the enthalpies of both the $2H_a$ and $2H_c$ phases of $MoSe_2$ up to 130 GPa. Figure 3 shows the enthalpy difference between the two phases. Unlike the case of MoS_2 where the enthalpies cross and the $2H_a$ polytype became more stable around 20 GPa [11], here the enthalpy difference actually *increases* with pressure, thus reinforcing the stability of the $2H_c$ structure. The slope of the enthalpy difference with increasing pressure (Fig. 3 and Fig. 2 in Ref. [11]) is equal to

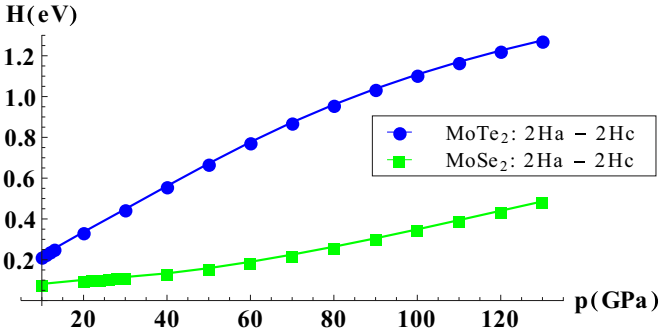

FIG. 3. (Color online) Pressure dependence of the enthalpy difference between the $2H_a$ and $2H_c$ structures of $MoSe_2$ and $MoTe_2$, respectively. Note the increase with pressure, indicating increased stability of $2H_c$ in both materials, unlike MoS_2 where $2H_a$ prevails at high pressure [11].

the volume difference between the respective phases, and the behavior of $MoSe_2$ and $MoTe_2$ is just the opposite of MoS_2: e.g., at $p = 20$ GPa, the volume of the unit cell of the $2H_a$ phase compared to the $2H_c$ one is larger in $MoSe_2$ and $MoTe_2$ by 0.2% and 1.4%, respectively, while in MoS_2, it is smaller by 1%. The layer-sliding structural transition observed in MoS_2, therefore, is not expected to occur in $MoSe_2$—and, as we shall see below, neither is it in $MoTe_2$.

We can rationalize the reason for that difference of behavior between $MoSe_2$ or $MoTe_2$ and MoS_2 based on simple considerations of interlayer Mo-Mo metallic bonding. We first note that only in the $2H_a$ structure are the Mo atoms in nearest layers vertically on top of one another, whereas they are staggered and chemically far away in $2H_c$. The $2H_a$ structure can be energetically favored if it can take advantage of d-electron propagation and metallicity along the c axis, such as is the case in NbS_2, $NbSe_2$, and high-pressure MoS_2. In $MoSe_2$ and $MoTe_2$, due to the larger radius of anions, the interlayer Mo-Mo distances are larger, e.g., by about 0.25 Å in $MoSe_2$ than in MoS_2. That makes interlayer d-electron propagation energetically less important in $MoSe_2$, leaving anion-anion repulsive forces in control of the enthalpy balance and, finally, favoring $2H_c$ over $2H_a$.

Having thus characterized the pressure evolution of the atomic structure, we can examine that of electronic properties, in particular the pressure-induced closing of band gap and metallization. The calculated PBE band structure is shown in Fig. 4 for $2H_c$-$MoSe_2$ at $p = 10$ and $p = 30$ GPa. The gap decreases with pressure at the rate of 0.026 eV/GPa. At $p = 10$ GPa, there still is an indirect band gap of 0.47 eV with the valence band top at the Γ point and the conduction band bottom at some point Q close to the midpoint between Γ and $K = \frac{1}{3}\mathbf{b}_1 + \frac{1}{3}\mathbf{b}_2$, where $\mathbf{b}_1, \mathbf{b}_2$ are reciprocal lattice vectors and $|\Gamma K| = \frac{4\pi}{3a}$.

At $p = 30$ GPa, the band gap is already closed and the valence and conduction bands exhibit a tiny overlap. Since the PBE approximation certainly does not overestimate the band gap, our calculation suggests that metallization of $2H_c$-$MoSe_2$ at lower pressures than 30 GPa is unlikely. This is compatible with the more recent resistivity data of Ref. [15] (which appear to correct earlier results [10] which had suggested a transition at 4 GPa for which there is no supporting evidence). In Fig. 5, we show our predicted pressure dependence of the band gap, which indicates metallization by band overlap in $MoSe_2$ at $P_{\text{met}} = 28$ GPa. Following band overlap, $2H_c$-$MoSe_2$ turns semimetallic with a low density of states at the Fermi level, as shown by Fig. 6 at $p = 30$ GPa. To establish an upper bound for the metallization pressure, we then performed calculations using the same structures, but with the HSE06 hybrid functional [22] in place of PBE, and found the gap closing at 40 GPa. Since this approximation is known to overestimate the band gap, we conclude that $MoSe_2$ metallizes at pressure between 28 and 40 GPa.

Since for an indirect band-gap semiconductor the exciton binding energy E_B remains finite right up to P_{met}, there is, in principle, the possibility upon gap closing to realize a so-called excitonic insulator state. That is a kind of charge-density-wave or spin-density-wave (SDW) state with wave vector $\mathbf{Q}$ theoretically predicted long ago in Ref. [23]. In a narrow range

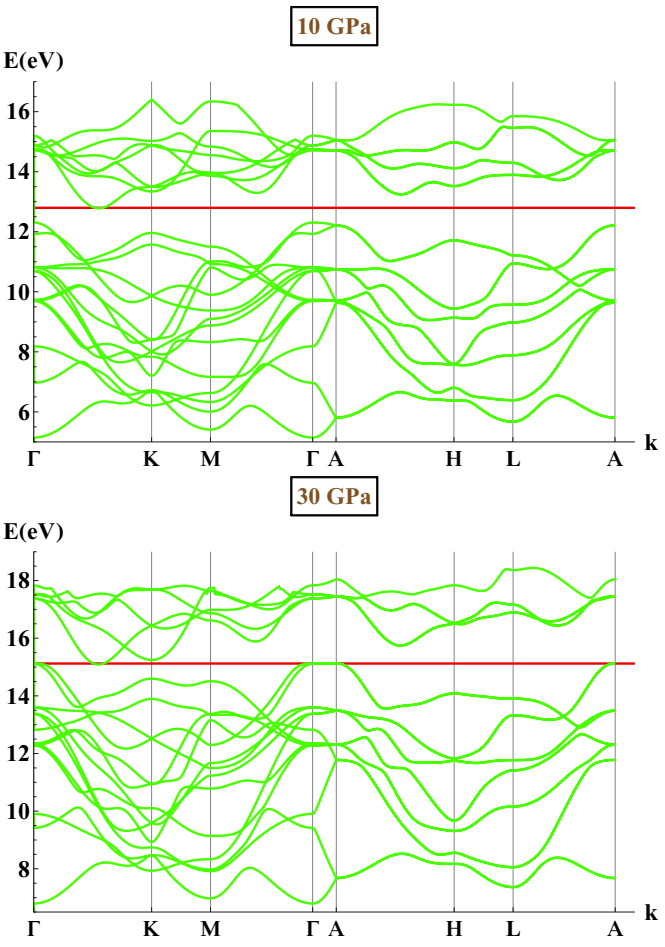

FIG. 4. (Color online) Band structure of $2H_c$-$MoSe_2$ at $p = 10$ GPa (upper panel) and $p = 30$ GPa (lower panel). Red line denotes the Fermi level.

of pressures immediately below P_{met}, the semiconducting gap becomes small enough to be comparable with the exciton binding energy E_B, expected here to be of the order of 10 meV. Given a gap reduction rate of 26 meV/GPa, this means that the excitonic state could exist in a narrow pressure range of about 4 kbar below P_{met}. The DFT-PBE electronic structure approximation does not properly treat the nonlocal exchange which is essential for the description of excitons, and thus

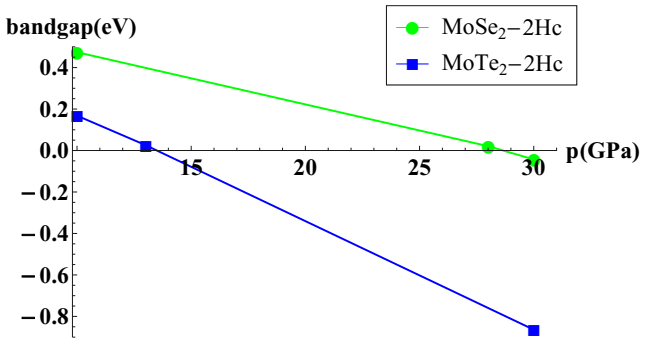

FIG. 5. (Color online) Pressure dependence of the band gap of $2H_c$-$MoSe_2$ and $2H_c$-$MoTe_2$.

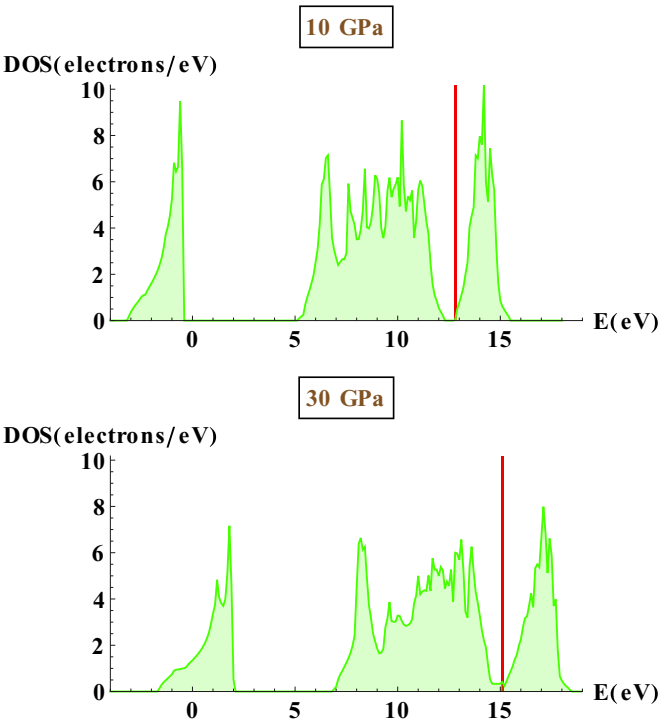

FIG. 6. (Color online) Density of states per unit cell of $2H_c$-$MoSe_2$ at $p = 10$ and $p = 30$ GPa. Red line denotes the Fermi level.

it does not describe excitonic insulator states. Therefore, we cannot make a quantitative prediction of the relevant portion of the pressure phase diagram and we must limit ourselves to a qualitative statement. The possible realization of this interesting state in MoS_2 was proposed in Ref. [11], but the structural transformation occurring at a pressure close to metallization presents a fatal complication in that system. From this point of view, $MoSe_2$ (and, as we shall see, $MoTe_2$), i.e., the structurally stable lattice in the metallization region, appears to be a more suitable system to search for an excitonic insulator state.

B. $MoTe_2$

Compared with $2H_c$-$MoSe_2$, there is much less experimental work for $2H_c$-$MoTe_2$ (α form), and we are not aware of either structure or resistivity data under pressure; our results represent a theoretical exploration. We carried out the same calculation protocol as for $2H_c$-$MoSe_2$: total-energy calculation, structural relaxation, enthalpy calculation, band structure and gap calculation. The calculated structural data are shown in Fig. 7. Here, too, the $2H_c$ structure remains stable under pressure, at least with respect to a transformation to $2H_a$. The enthalpy difference stabilizing $2H_c$ over the $2H_a$ structure shown in Fig. 3 is even stronger here than in $MoSe_2$, in agreement with our earlier explanation involving the volume difference between the phases and the larger radius of Te anions relative to Se.

Figure 8 shows the band structure of $2H_c$-$MoTe_2$. Here we took special care to verify that the spin-orbit interaction has no major effect on the states in the vicinity of the Fermi level. At 10 GPa, there is still a small but finite band gap. At 13 GPa,

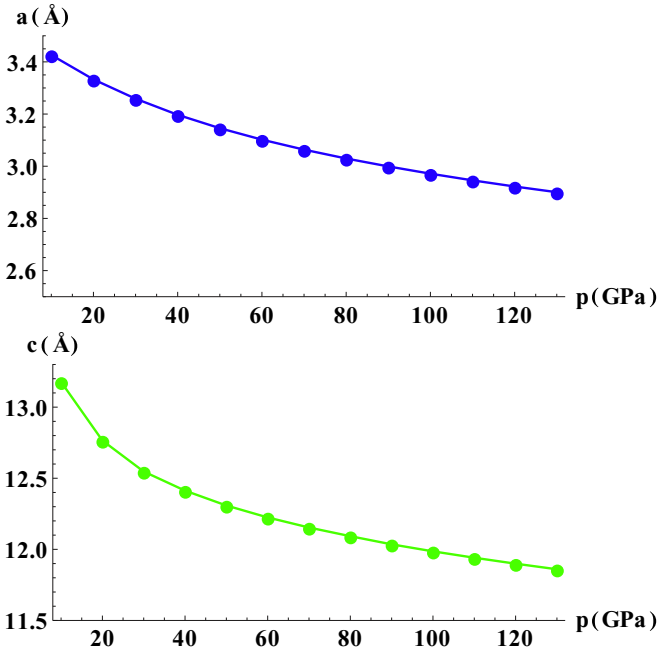

FIG. 7. (Color online) Pressure dependence of the calculated lattice parameters a (upper panel) and c (lower panel) of $2H_c$-$MoTe_2$.

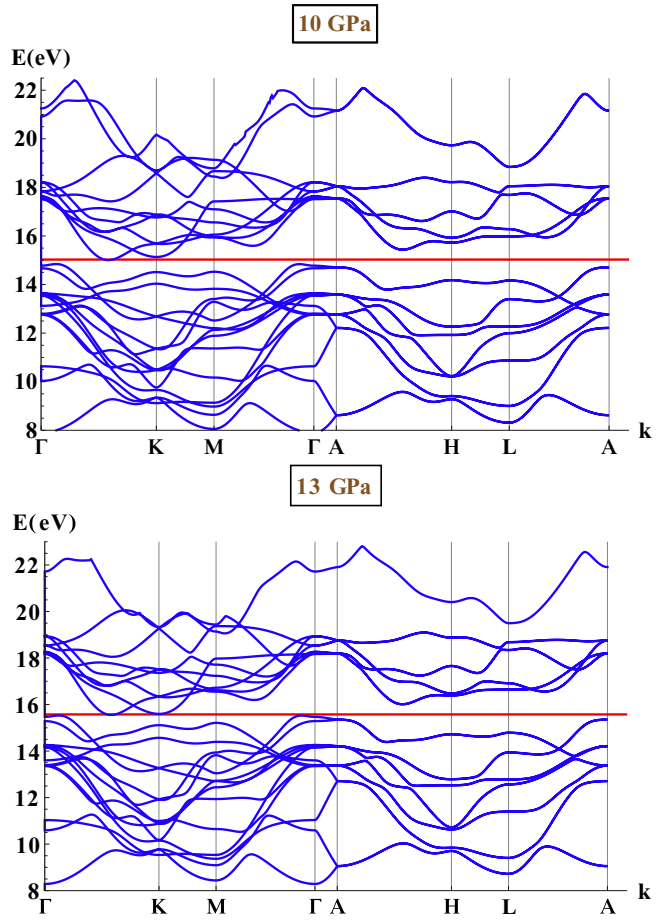

FIG. 8. (Color online) Band structure of $2H_c$-$MoTe_2$ at $p = 10$ GPa (upper panel) and $p = 13$ GPa (lower panel). Red line denotes the Fermi level.

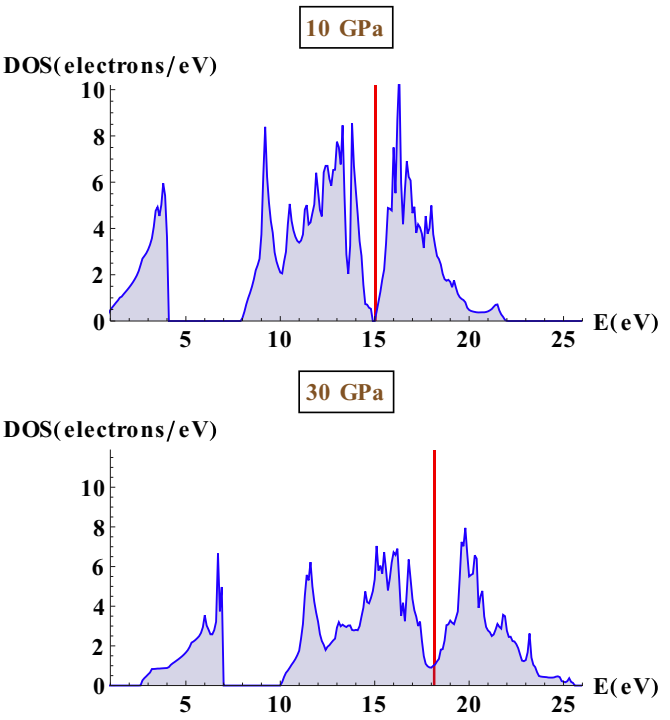

FIG. 9. (Color online) Density of states per unit cell of $2H_c$-$MoTe_2$ at $p = 10$ and $p = 30$ GPa. Red line denotes the Fermi level.

band overlap has already taken place between the valence band top, now slightly displaced from Γ, and the conduction band bottom, which has two nearly degenerate minima—one again close to midpoint Q between Γ and K points and another one at the K point. Thus, even in $2H_c$-$MoTe_2$, there could be a narrow excitonic insulator phase just below the metallization pressure; however, the CDW or SDW condensate wave vector is less straightforward to predict. Figure 9 shows the electronic density of states at 10 and 30 GPa, and one can see that even at 30 GPa, which is more than twice the metallization pressure, the electronic DOS remains rather low, indicating semimetallicity. Here again we performed a hybrid functional [22] calculation and found gap closing at 19 GPa, thus placing the metallization pressure of $2H_c$-$MoTe_2$ between 13 and 19 GPa.

Finally, we studied the metastable β form of $MoTe_2$ (Fig. 10), which is already metallic at zero pressure. The

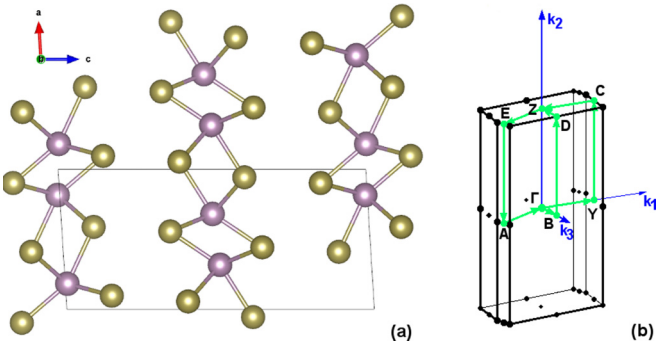

FIG. 10. (Color online) Structure of (a) the β form of $MoTe_2$ and (b) its Brillouin zone.

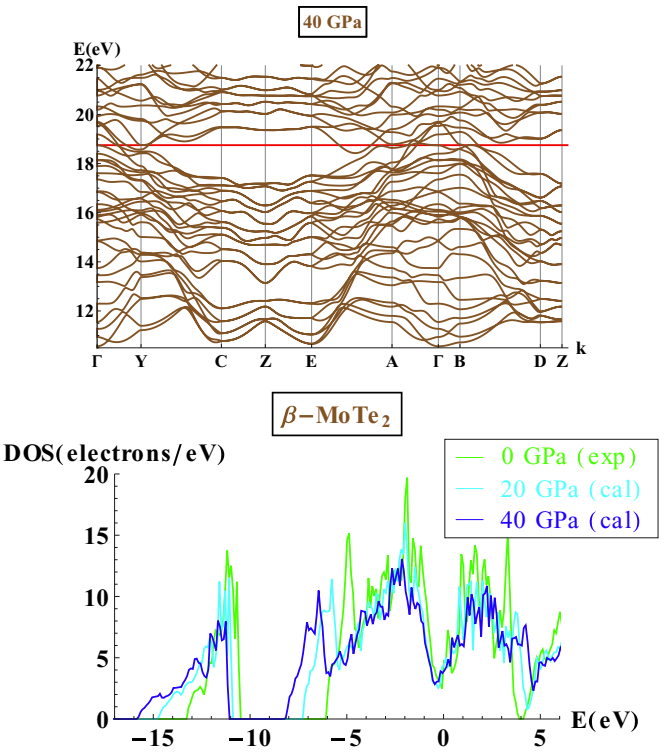

FIG. 11. (Color online) Band structure of β-$MoTe_2$ at $p = 40$ GPa (upper panel) and density of states (per unit cell) at $p = 20$ and $p = 40$ GPa and for the experimental unit cell at normal conditions (lower panel). In the band structure graph the red line denotes the Fermi level. In the DOS graph, the Fermi level is at zero.

enthalpy of this form at 20 GPa is higher by 0.12 eV ($MoTe_2$ group) than that of the $2H_c$ form. In order to check how the metallicity of this phase evolves with pressure, we compressed and relaxed this metastable structure to 20 and 40 GPa and recalculated the electronic DOS (Fig. 11). The band structure at 40 GPa is also shown in Fig. 11. Comparing the DOS under pressure to that calculated for the experimental cell at normal conditions [17], we see that the effect of pressure again does not raise the DOS at the Fermi level very much. This suggests that pressure is not a likely tool for a major increase of metallicity, and of BCS superconductivity, of β-$MoTe_2$.

IV. CONCLUSIONS

The structural and electronic properties of $MoSe_2$ and $MoTe_2$ are studied theoretically under high pressure. Unlike MoS_2, these TMD layered compounds are not prone to a layer-sliding transition from $2H_c$ to the $2H_a$ polytype. Since $MoSe_2$ is also a good lubricant, as is MoS_2 [24], one can conclude that easy interlayer sliding in the high-pressure pristine crystals may not be directly related to the lubricity shown by the technical emulsions based on these materials. Based on DFT-PBE and HSE06 calculations, both compounds are predicted to metallize via closing of an indirect gap and consequent band overlap at pressures between 28 and 40 GPa ($2H_c$-$MoSe_2$) and 13 and 19 GPa ($2H_c$-$MoTe_2$). Beyond the metallization point, they should behave as semimetals, retaining a low density of states at the Fermi level. Even in the metastable β-$MoTe_2$ phase, which is metallic already at zero pressure, compression does not appear to increase metallicity substantially. Therefore, neither $MoSe_2$ nor $MoTe_2$ seem likely, in their pristine nonintercalated state, to become good BCS superconductors in the range of pressures considered. Weak superlattice structural and electronic extra Bragg spots should be looked for just below the metallization pressure, with their possible presence providing evidence of an excitonic insulator or CDW phase. In that case, enhanced superconductivity could arise in the metallic phase following the CDW at higher pressures, as seen for example in 1T-$TiSe_2$ [25].

ACKNOWLEDGMENTS

M.R. was supported by the Slovak Research and Development Agency under Contract No. APVV-0036-11. R.M. was supported by the Slovak Research and Development Agency under Contract No. APVV-0558-10 and by the Project Implementation No. 26220220004 within the Research & Development Operational Programme funded by the ERDF. Part of the calculations was also performed in the Computing Centre of the Slovak Academy of Sciences using the supercomputing infrastructure acquired in Projects No. ITMS 26230120002 and No. 26210120002 (Slovak infrastructure for high-performance computing) supported by the Research & Development Operational Programme funded by the ERDF. Work in Trieste was partly sponsored by EU-Japan Project LEMSUPER, Sinergia Contract No. CRSII2$_1$36287/1, and ERC Advanced Grant No. 320796-MODPHYSFRICT.

[1] J. Wilson and A. Yoffe, Adv. Phys. **18**, 193 (1969).
[2] L. Gmelin, *Gmelin Handbook of Inorganic and Organometallic Chemistry* (Springer-Verlag, Berlin, 1995), Vol. B 7–9, p. 16.
[3] K. F. Mak, C. Lee, J. Hone, J. Shan, and T. F. Heinz, Phys. Rev. Lett. **105**, 136805 (2010).
[4] J. Feng, X. Qian, C.-W. Huang, and J. Li, Nat. Photon. **6**, 866 (2012).
[5] Q. Yue, J. Kang, Z. Shao, X. Zhang, S. Chang, G. Wang, S. Qin, and J. Li, Phys. Lett. A **376**, 1166 (2012).
[6] S. M. Tabatabaei, M. Noei, K. Khaliji, M. Pourfath, and M. Fathipour, J. Appl. Phys. **113**, 163708 (2013).
[7] P. Lu, X. Wu, W. Guo, and X. C. Zeng, Phys. Chem. Chem. Phys. **14**, 13035 (2012).
[8] H. Shi, H. Pan, Y.-W. Zhang, and B. I. Yakobson, Phys. Rev. B **87**, 155304 (2013).
[9] R. Aksoy, E. Selvi, and Y. Ma, J. Phys. Chem. Solids **69**, 2138 (2008).
[10] M. Dave, R. Vaidya, S. G. Patel, and A. R. Jani, Bull. Mater. Sci. **27**, 213 (2004).

[11] L. Hromadová, R. Martoňák, and E. Tosatti, Phys. Rev. B **87**, 144105 (2013).
[12] R. Aksoy, Y. Ma, E. Selvi, M. C. Chyu, A. Ertas, and A. White, J. Phys. Chem. Solids **67**, 1914 (2006).
[13] T. Livneh and E. Sterer, Phys. Rev. B **81**, 195209 (2010).
[14] N. Bandaru, R. S. Kumar, D. Sneed, O. Tschauner, J. Baker, D. Antonio, S.-N. Luo, T. Hartmann, Y. Zhao, and R. Venkat, J. Phys. Chem. C **118**, 3230 (2014).
[15] S. H. Chaki, G. K. Solanki, A. J. Patel, and S. G. Patel, High Press. Res. **28**, 133 (2008).
[16] B. E. Brown, Acta Crystallogr. **20**, 268 (1966).
[17] W. G. Dawson and D. W. Bullett, J. Phys. C: Solid State Phys. **20**, 6159 (1987).
[18] The XCrySDen program (A. Kokalj, Comput. Mater. Sci. **28**, 155 (2003), http://www.xcrysden.org) was used to visualize the path in Brillouin zone in Figs. 1(c) and 10(b).
[19] J. P. Perdew, K. Burke, and M. Ernzerhof, Phys. Rev. Lett. **77**, 3865 (1996).
[20] P. Giannozzi, S. Baroni, N. Bonini, M. Calandra, R. Car, C. Cavazzoni, D. Ceresoli, G. L. Chiarotti, M. Cococcioni, I. Dabo *et al.*, J. Phys. Condens. Matter **21**, 395502 (2009).
[21] H. J. Monkhorst and J. D. Pack, Phys. Rev. B **13**, 5188 (1976).
[22] J. Heyd, G. E. Scuseria, and M. Ernzerhof, J. Chem. Phys. **124**, 219906 (2006).
[23] D. Jérome, T. M. Rice, and W. Kohn, Phys. Rev. **158**, 462 (1967).
[24] J. F. Yang, B. Parakash, J. Hardell, and Q. F. Fang, Front. Mater. Sci. **6**, 116 (2012).
[25] A. F. Kusmartseva, B. Sipos, H. Berger, L. Forró, and E. Tutiš, Phys. Rev. Lett. **103**, 236401 (2009).
[26] Mo.pbe-spn-kjpaw_psl.0.2.UPF, Se.pbe-n-kjpaw_psl.0.2.UPF and Te.pbe-dn-kjpaw_psl.0.2.2.UPF from http://www.quantum-espresso.org.
[27] Mo.pbe-mt_fhi.UPF, Se.pbe-mt_fhi.UPF and Te.pbe-mt_fhi.UPF from http://www.quantum-espresso.org.